EDL Simulation Results for the Mars 2020 Landing Site Safety Assessment

David Way
NASA Langley Research Center
Hampton, VA 23681-2199
757-864-8149
david.w.way@nasa.gov

Soumyo Dutta
NASA Langley Research Center
Hampton, VA 23681-2199
757-864-3894
soumyo.dutta@nasa.gov

Carlie Zumwalt
NASA Langley Research Center
Hampton, VA 23681-2199
757-864-5891
carlie.h.zumwalt@nasa.gov

Samalis Santini De León
Texas A&M University
College Station, TX
ssantini@tamu.edu

***Abstract*—The Mars 2020 rover is NASA's next flagship mission, set to explore Mars in search of scientific evidence of past microbial life. Importantly, the rover will also, for the first time, have the ability to collect and cache rock and soil samples for retrieval and return to laboratories here on Earth.**

A key step in the development of the Mars 2020 mission is the selection of a suitable landing site with the largest likelihood of meeting scientific goals. This decision is a complex and critical one that requires close interaction between the scientific and engineering communities. The chosen landing site must be both scientifically interesting — providing the project with the greatest possible chance of gathering credible and defendable scientific evidence — and also safe enough to attempt a landing in the first place. Thus, arguably one of the most important undertakings of the Entry, Descent, and Landing (EDL) team, is to effectively enumerate, quantify, and communicate the landing risks to all of the stakeholders. The culmination of this effort is the Landing Site Safety Assessment, which is a review commissioned by the project, presided over by the EDL Standing Review Board, and attended by management and science stakeholders, in which the EDL team communicates their assessment of the associated landing risks and the statistical probability of a successful landing at each of the final candidate landing sites.

This paper summarizes the results of high-fidelity computer simulations of the Mars 2020 EDL sequence used in this assessment. From an EDL performance perspective, all four candidates offer similar level of robustness, which is in-family with Mars Science Laboratory (MSL). However, two new features of the Mars 2020 EDL sequence – range trigger and Terrain-Relative Navigation (TRN) – dramatically enhance the capability of the EDL system to safely land at landing sites with much more rugged terrain than ever before considered. This has allowed the landing site selection for Mars 2020 to proceed in a manner that has been unprecedentedly weighted more heavily toward scientific interest and less heavily on engineering constraints. With TRN, the overall probability of success is predicted to be approximately 99% for all of the candidates.

TABLE OF CONTENTS

[1] IEEE Aerospace Conference #2501, Version 2, Updated January 1, 2020.

1. INTRODUCTION

On November 19, 2018, NASA announced that Jezero Crater had been selected as the landing site for the Mars 2020 rover. This announcement marked the end of a four-year process to choose where the rover will land when it arrives at Mars, February 18, 2021.

Since 2014, members of the project, along with scientists from around the world, have met four times to identify and discuss the merits of potential landing sites. As many as 27 sites have been identified, discussed, and ranked. By the third workshop that number was reduced to only three (though a fourth would be added later). The fourth and final landing site workshop convened October 16, 2018, to evaluate the merit of the remaining sites and provide a recommendation to NASA's Science Mission Directorate for which single landing site best meets the scientific objectives of the mission. That recommendation, along with an evaluation of the safety and performance of the vehicle at each landing site, was used to down-select from four potential sites to the final chosen one.

In preparation for the final landing site workshop, the Entry Descent and Landing (EDL) team met with members of the EDL Standing Review Board (SRB) to provide an assessment of the vehicle's ability to execute a safe landing at each of the four candidate landing sites. It was the responsibility of the SRB, which evaluates EDL system design across the project life-cycle, to vet that assessment. The primary objective of the review was to address the relative safety ranking of the sites and to determine, from an EDL risk perspective, if any of the four sites should be removed from contention. Consideration was also given to the likelihood of that assessment changing as additional information is provided by future studies, system tests, or parameter tuning.

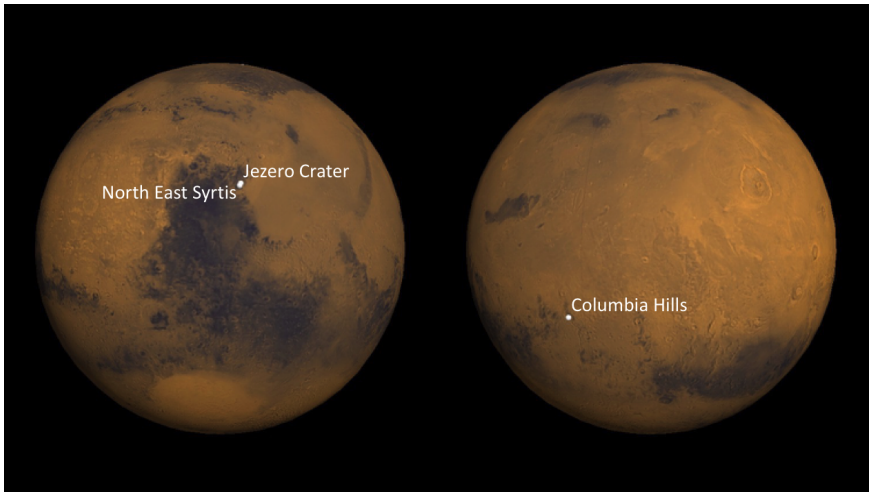

Figure 1. Top three Mars 2020 candidate landing sites from the 3rd Landing Site Workshop in 2017. Image Credit: NASA

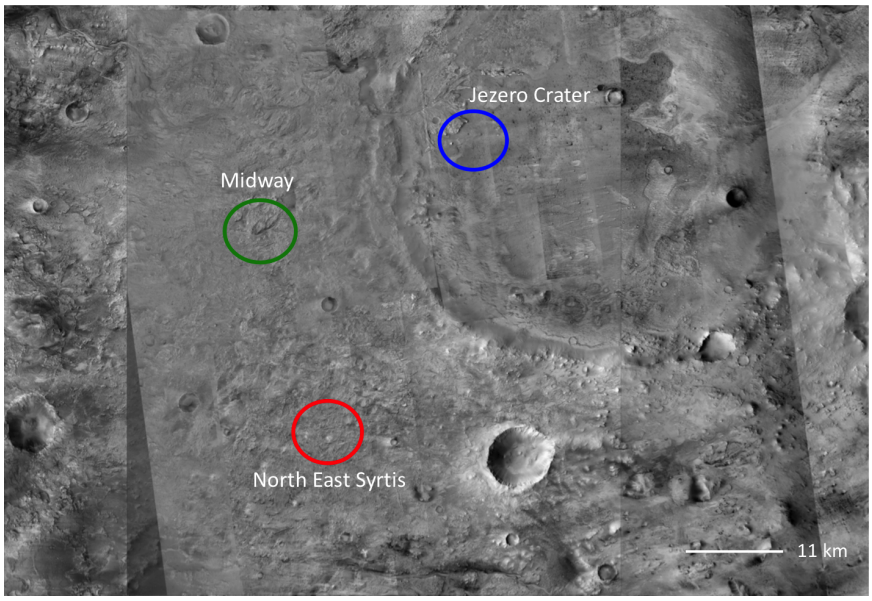

Figure 2. Proximity of three Syrtis Major landing sites. Rover operators have identified traversable paths between Jezero Crater and Midway, thus establishing the feasibility of a dual-site mission. Image Credit: NASA

Table 1. Mars 2020 Final Four Candidate Landing Sites

Airport Code	Landing Site Name	Lat. (^oN)	Lon. (^oE)	Elev. (km)
CLH	Columbia Hills	-14.5711	175.4374	-1.920
JEZ	Jezero Crater	18.4463	77.4565	-2.566
MDW	Midway	18.2747	77.0481	-2.013
NES	North East Syrtis	17.8899	77.1599	-2.032

2. LANDING SITE CANDIDATES

Following the third Landing Site Workshop, held in Monrovia, CA, on February 8-10, 2017, the project down-selected three final candidates from a short list of eight landing sites. Figure 1 shows the location of these sites on Mars. Subsequent to that meeting, the EDL team was asked to evaluate a potential fourth landing site (named "Midway"), for reasons that will be explained later. Table 1 lists the latitude and longitude of each landing site, along with the elevation above the Mars Orbiting Laser Altimeter (MOLA) reference areoid. Notably, only 646 m of elevation separates all four landing sites. Because of this, we should expect very similar EDL performance at each site. The "airport code" listed in the first column of Table 1 is a three-letter, short-hand notation traditionally used by the EDL systems analysis team. The following section briefly introduces each of these sites.

Jezero Crater (JEZ)

Jezero Crater is a Northern hemisphere impact crater, approximately 45 km in diameter, located in the North East portion of the Syrtis Major quadrangle along the Western edge of Isidis Planitia, just South of Nilli Fossae. The most prominent feature of the crater is a channel, cut through the Western crater wall, which leads to an impressive fan delta – indicating that the ancient crater once contained a lake. On Earth, such environments are very favorable for concentrating

and preserving signs of life. A portion of the Eastern edge of this delta is contained within the landing ellipse and includes a steep face, where the delta has been eroded away with approximately $80\ m$ of vertical elevation relief. However, the primary landing hazard throughout the ellipse is the presence of rocks.

North East Syrtis (NES)

As the name implies, North East Syrtis is a site located in the North Eastern region of Syrtis Major Planum in the Syrtis Major quadrangle, near the Western edge of Isidis Planitia, and South West of Jezero Crater. Like Jezero, North East Syrtis is also located in the Northern Hemisphere at approximately $18\ deg$ latitude. The ellipse features layered terrain and large blocks of megabreccia that scientists believe may have been formed by underground mineral springs and could have been hospitable to life. Not as generally rocky as Jezero Crater, the primary hazard here are steep slopes associated with eroded mesas scattered throughout the ellipse. Additionally, these slopes are often accompanied by smaller rocks.

Midway (MDW)

Jezero Crater and North East Syrtis offer two completely different environments that could have favored, and recorded, the development of microbial life on Mars at the same time that it was developing here on Earth. The close proximity of these sites (approximately $37\ km$) has raised the possibility of a dual-site mission, whereby the rover would land in one of these sites and drive to the other. However, this distance is likely too far to make this option feasible. Therefore, an additional site was identified that is roughly half-way between Jezero Crater and North East Syrtis. This new site, which is being called "Midway", is located approximately $25\ km$ South West of Jezero Crater, thus making a dual-site mission much more feasible. Figure 2 illustrates the close proximity of the three Syrtis Major landing sites. The geology and science value at Midway is expected to be similar to that of North East Syrtis. Thus, a dual-site mission would land at either Jezero Crater or Midway and drive to the other. The current ellipse for Midway is centered around a channel that provides tens of meters of vertical relief.

Columbia Hills (CLH)

Columbia Hills is the highest elevation of the four candidates and is the only site located in the Southern hemisphere. It is a series of low hills located in Gusev crater, within the Aeolis quadrangle, and is the same site explored by the MER-A *Spirit* rover. This site is hypothesized to be an ancient hot-springs environment, which could harbor signs of microbial life. Because of the reconnaissance conducted by the *Spirit* rover, much is already known about this site at scales smaller than can be observed from orbit. Columbia Hills also has the smallest distribution of relief out of all four sites as the location is generally very flat.

3. PERFORMANCE RELATIVE TO MSL

The Mars 2020 EDL system derives its heritage from the Mars Science Laboratory (MSL) landing. Because of the similarity between the two missions, this landing provides an excellent benchmark for Mars 2020 EDL system performance. On 5 August, 2012, the *Curiosity* rover successfully landed in Gale Crater at an elevation of $-4.5\ km$ relative to the MOLA areoid. Compared to the assessed maximum altitude capability of approximately $0\ km$ MOLA, this low landing site elevation provided roughly $45\ s$ of additional timeline margin[2] above acceptable minimums. The actual as-flown timeline margin observed in flight was $62.5\ s$.

For context, this feat was also accomplished in a very unfavorable opportunity. The geometry of the 2011 Mars launch opportunity resulted in an arrival at a solar longitude of $L_S = 150.7°$, which is very near the lowest extrema in the seasonal surface pressure cycle. In contrast, the Mars 2020 launch opportunity arrives at $L_S = 5.6°$, which is near the high in the pressure cycle. Thus, because Gale Crater was not challenging from an elevation perspective and also because the 2020 launch opportunity arrives in a very favorable season, the Mars 2020 project is able to use the same EDL architecture to land more mass at nearly $2.6\ km$ higher elevation, with only a very modest decrease in timeline margin, if any.

The terminal velocity on a $21.5m$ parachute for an MSL-class vehicle provides us with a useful thumb rule. Approximately $1\ s$ of timeline margin is lost for every $100\ m$ of increased landing site elevation. From this thumb rule, we would expect a loss of approximately $26\ s$ of timeline margin, relative to landing in Gale Crater. Likewise, a traditional performance thumb rule[3] of $100\ m$ of altitude loss per 1% increase in entry mass would predict an additional loss of $800\ m$ and $8\ s$ of timeline associated with the 8% increase in entry mass (approximately $250\ kg$), relative to MSL.

However, previous analysis has demonstrated that the expected increase in altitude performance associated with the change in arrival season is approximately $1500\ m$, equivalent to an additional $15\ s$ increase in timeline margin. Another improvement in timeline comes from retargeting parachute deployment to a slightly higher Mach number. Mars 2020 will target a mean Mach number of 1.75, whereas MSL targeted 1.70. From yet another EDL thumb rule ($800\ m$ per 0.10 change in Mach number) this modest increase of 0.05 results in approximately $400\ m$ of additional altitude and $4\ s$ of additional timeline.

All together, these thumb rules would predict an overall decrease in timeline margin of around $15\ s$. The high-fidelity simulation results support a mean reduction of approximately $13\ s$ when comparing MSL and CLH, the highest of the four proposed landing sites. Thus, our rough EDL performance thumb rules produce reasonable approximations that are beneficial in understanding the relative contributions of each of the factors: landing site elevation, entry mass, arrival season, and parachute deploy tuning.

Importantly, this modest decrease of only $13\ s$ from the previously observed $62.5\ s$ of timeline margin still provides ample timeline at all of the proposed Mars 2020 landing sites. Thus, as will be shown in more detail later, the design, tuning, margins, and performance of the Mars 2020 EDL system are all in-family with MSL heritage and are not particularly stressing, even considering the increased mass and landing site elevation.

[2] Timeline margin is defined by the EDL team as the time between establishing a valid radar solution prior to the first event requiring a valid radar altitude (MLE priming).

[3] Attributed to Gil Carman of the Johnson Space Center

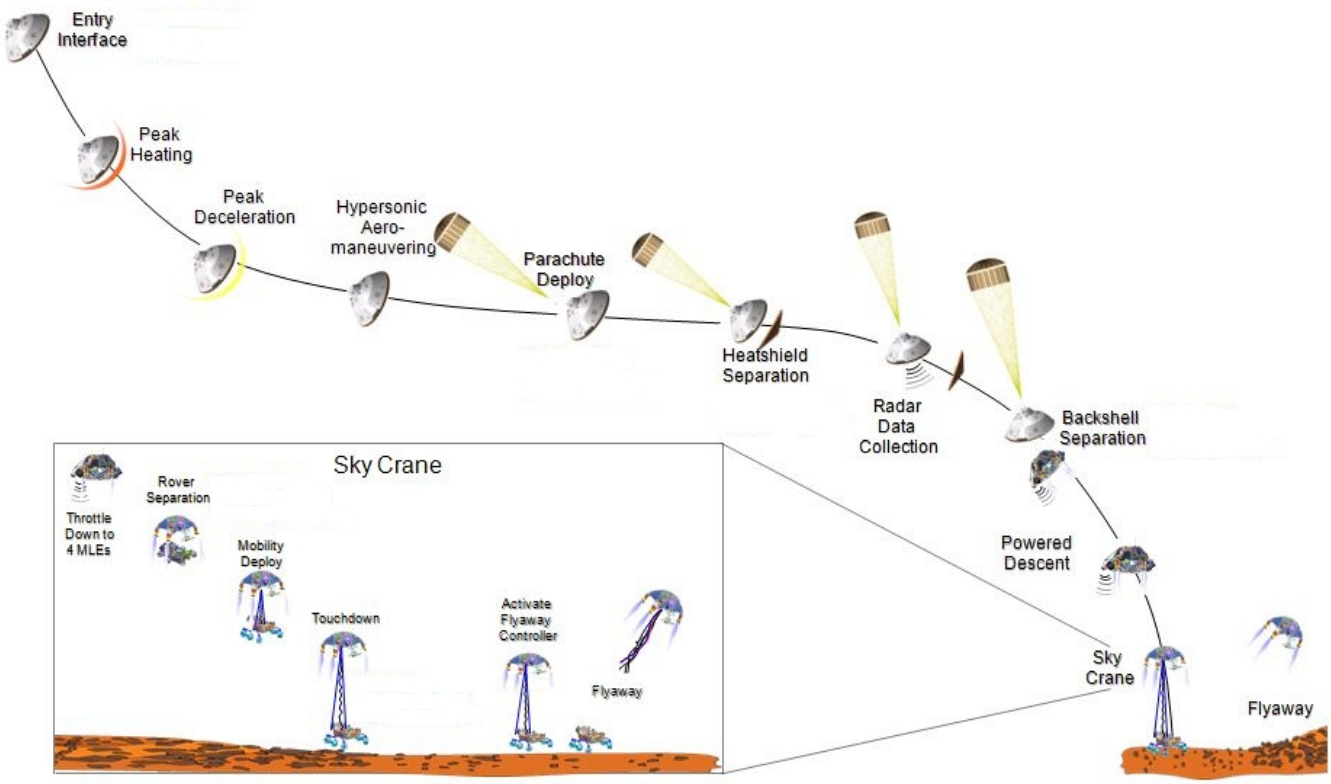

Figure 3. Mars Science Laboratory (MSL) Entry, Descent, and Landing (EDL) Sequence. Image Credit: NASA/JPL-Caltech

4. NEW EDL FEATURES

On the whole, the Mars 2020 EDL sequence is very nearly an exact copy of MSL, which is depicted in Figure 3. Two major exceptions to this statement are a change to the algorithms that initiate the Straighten-Up and Fly Right (SUFR) maneuver and the addition of a Terrain-Relative Navigation (TRN) system. Taking these two changes collectively, they dramatically enhance the capability of the EDL system to safely land at landing sites with much more rugged terrain than ever before considered. This has allowed the landing site selection for Mars 2020 to proceed in a manner that has been unprecedentedly weighted more heavily toward scientific interest and less heavily on engineering constraints. As a result, Mars 2020 will be the most daring landing ever attempted on Mars.

Terrain-Relative Navigation (TRN)

The goal of the TRN system is to improve the position knowledge of the spacecraft so that a precise landing location can be chosen for a safe touchdown. The Mars 2020 implementation of the TRN system is decomposed into two separate subsystems with independent functions: the Lander Vision System (LVS) and Safe Target Selection (STS). The function of LVS is to provide an accurate localization of the vehicle's position relative to observable landmarks on the surface of Mars. Once the local position is known, the function of STS is to choose the exact location to execute the vertical portion of the powered descent profile, along with the Sky Crane landing.

LVS performs its localization function by acquiring real-time images of the scenery during parachute descent. It then compares landmarks in those images with an on-board map of the landing site. The on-board mosaic image is constructed from orbital images at $6\ m/pixel$ resolution, acquired by the MRO Context (CTX) camera. By matching landmarks and correlating the real-time images to this map, LVS determines the three-dimensional position and attitude of the Lander Vision Camera (LCAM) to within $40\ m$ of horizontal position – by requirement. However, it is estimated from field testing that the actual performance of the system could approach $20\ m$ of accuracy.

Given the LVS position estimate, the STS system consults another on-board data product, the Safe Targets Map (STM), to select the final landing target from within a region that meets all of the constraints placed on the powered approach divert: a minimum divert distance to minimize the risk of re-contact with the parachute and backshell, a maximum divert distance to stay within budgeted fuel use, and a maximum throttle setting to reserve thrust margin for attitude control. These requirements are met by two wedge-shaped regions, each $137,000\ m^2$ in area (approximately $34\ acres$) – one to the left and one to the right of the vehicle's estimated ground track. Each wedge is formed by a minimum radius arc of $300\ m$, a maximum radius arc of $635\ m$, and an arc-length of $50\ deg$ ($\pm 25\ deg$). Landing locations outside of this wedge, including those within $300\ m$ of the "zero-divert point", are not considered under any circumstances.

Like the LVS map, the on-board STM covers the entire landing region at $10\ m$ per pixel resolution. Each pixel is assigned an integer "safety level" based on the aggregate risk of touchdown failure associated with: the slope of the terrain, known larger rocks identified from orbital imagery, the estimated Cumulative Fractional Area (CFA) of smaller rocks, and inescapable hazards (such as steep-walled craters or rippled sand fields). Importantly, these hazards are also

Table 2. Mars 2020 Footprint Comparison

Parameter	Range Trigger	Vel. Trigger	Diff.
Major Axis ($2a$)	7.11 km	11.10 km	-35.9%
Minor Axis ($2b$)	6.53 km	6.37 km	+2.5%
Area (πab)	36.48 km^2	55.55 km^2	-34.3%

buffered in a way that ensures a safe stand-off distance based on expected targeting accuracy.

STS selects the STM pixel with the maximum safety level in each of the two wedges. Then, the exact same logic that determined the direction of the divert for MSL is re-used to designate which of these two targets is the primary target. The primary target is used unless the reverse target is determined to be more safe by a minimum threshold of safety levels. This feature provides a risk-risk trade-off between landing hazards and the possibility of recontact with the backshell and parachute.

Thus, through *in-situ* sensing (descent camera images), the TRN system is able to selectively choose a landing target that maximizes the probability of avoiding known hazards that can be identified *a priori* from orbital imagery. It is important to note, however, that the Mars 2020 TRN system does not include Hazard Detection and Avoidance (HDA) functionality. The Mars 2020 system is not capable of actively detecting and avoiding hazards that haven't been identified from orbit, and therefore, aren't included in the STM.

Range Trigger

The Mars 2020 project has adopted a change to the algorithm that triggers the SUFR maneuver, which initiates the parachute deployment sequence. For MSL, this event utilized a velocity trigger – meaning that the event was executed when the navigated velocity dropped below a particular set-point. For Mars 2020, the SUFR event is now activated by a range trigger – meaning that the event is now triggered when the estimated range-to-go drops below a particular set-point (currently $16,000\ m$).

For a velocity trigger, dispersions in planet-relative velocity are minimized by design, but this trigger results in large landing footprints due to under-shooting or over-shooting the landing target while waiting to slow down. Conversely, a range trigger minimizes downrange dispersions, and thus footprint size, but does so at the expense of larger velocity dispersions. During MSL development, a range trigger was considered, but not selected due to concerns of higher parachute deploy Mach numbers while trying to maintain maximum altitude performance. Way [2] provides a detailed side-by-side comparison between range and velocity triggers and also describes a wind correlation that minimizes Mach number spread in the case of a range trigger, in spite of the increased spread in planet-relative velocity.

When there exists sufficient margins with respect to allowable parachute deploy conditions (e.g. Mach number, dynamic pressure, and altitude), the use of a range trigger can significantly reduce the size of the landing footprint. However, the actual magnitude of this reduction is unique to each situation and depends on the relative contributions of other modeled dispersions [3].

Table 2 quantifies the reduction in footprint size for a range

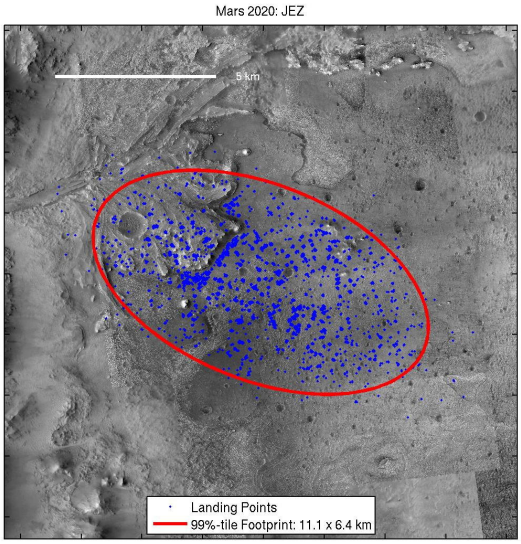

Figure 4. 8000 Monte Carlo landing points at the Jezero Crater landing site, using a velocity trigger. The size of the 99%-tile ellipse is 11.1 x 6.4 km.

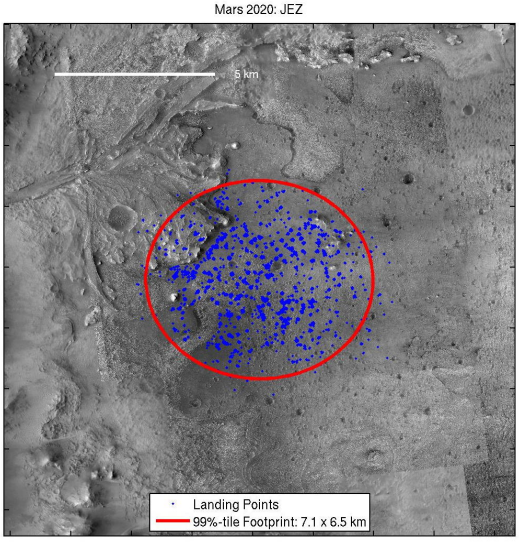

Figure 5. 8000 Monte Carlo landing points at the Jezero Crater landing site, using a range trigger. The size of the 99%-tile ellipse is 7.1 x 6.5 km.

trigger, relative to that of a velocity trigger, for the Mars 2020 EDL system – a reduction of approximately 34% in total area. Figures 4 and 5 further illustrate the very noticeable change in footprint size. The effect of this reduction on landing site selection is to allow smaller regions to be proposed as landing site candidates, and to place the center of those regions closer to scientifically interesting targets. Not only is the area of terrain that must be analyzed and be relatively free of hazards smaller, but the size of the on-board maps that must be carried for TRN can be smaller and rover drive times to scientific targets of interest are also reduced. Figure 6 compares the 99%-tile touchdown footprints, with range trigger, at all four of the candidate landing sites. These ellipses are approximately circular with a diameter of around 7 km.

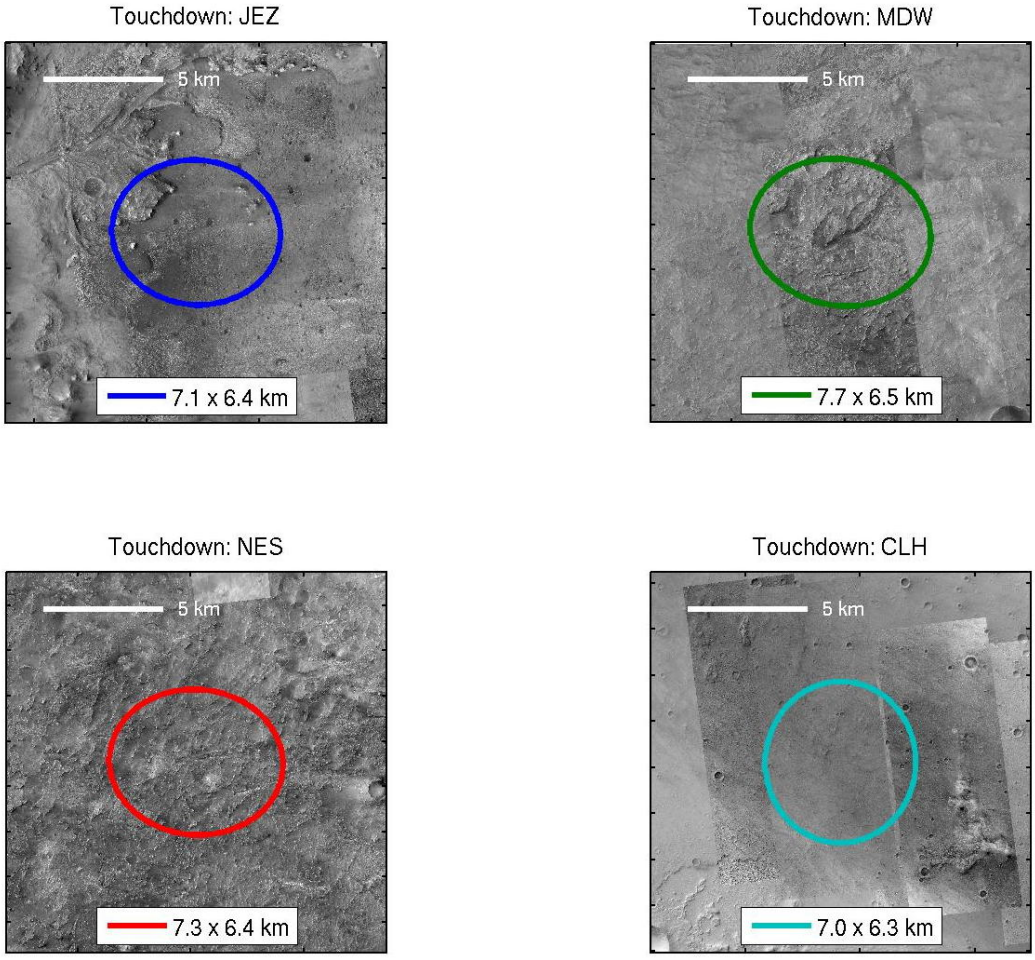

Figure 6. Comparison of touchdown footprints at candidate landing sites. Ellipses are 99%-tile.

5. PERFORMANCE WALKTHROUGH

The following section provides a brief walk-through of the Mars 2020 EDL system performance, organized roughly by timeline. These results demonstrate that the Mars 2020 EDL performance is similar to, and in family with, MSL EDL performance. Additionally, performance metrics across all four landing sites show very little differentiation among the candidates. With TRN, the calculated probability of succcess[4] is approximately 99% for all four sites. However, the perceived risk at each site is not equivalent, as will be discussed later.

In the following subsections, both box-and-whisker plots and quantile-quantile (q-q) plots are used to compare the results of Monte Carlo simulations across all four landing sites as well as to MSL day-of-entry predictions (e.g. Figure 7). Where appropriate, the MSL as-flown reconstruction value is also shown. In all cases, the statistics are based on a sample size of 8001. For the box-and-whisker plots, the blue "box" depicts results from the middle-50% of cases – between the the 25th percentile and the 75th percentile. The black "whiskers" denote the 1%-tile and 99%-tile, thus the middle 98%. The red line in the middle of the box is the 50th percentile (median value). The same data set is also portrayed in the q-q plots. For these plots, the Monte Carlo samples are sorted and assigned a quantile. An equivalent quantile of a standard normal distribution is then found from the inverse of the Gaussian Cumulative Distribution Function (CDF). The data quantiles are then plotted against the normal quantiles to compare the shape of the statistical distribution. All 8001 cases are plotted, clearly indicating any outliers. For some metrics, where the metric is one-sided, a Rayleigh distribution is used in lieu of a normal.

[4]The probability of success discussed here includes only the hazards associated with survivability of the system's interaction with the terrain at the moment of touchdown. Specifically, it does not include any probabilistic risk assessment of successfully executing the EDL sequence nor any estimate of the likelihood of either a hardware or software failure.

Table 3. Mean Entry Interface (EI) Conditions

Parameter	Symbol	Value
Radius	r_{EI}	3522.2 km
Flight path angle	γ_{EI}	-15.5 deg
Velocity	V_{EI}	5.4 km/s
Mass	m_{EI}	3406 kg

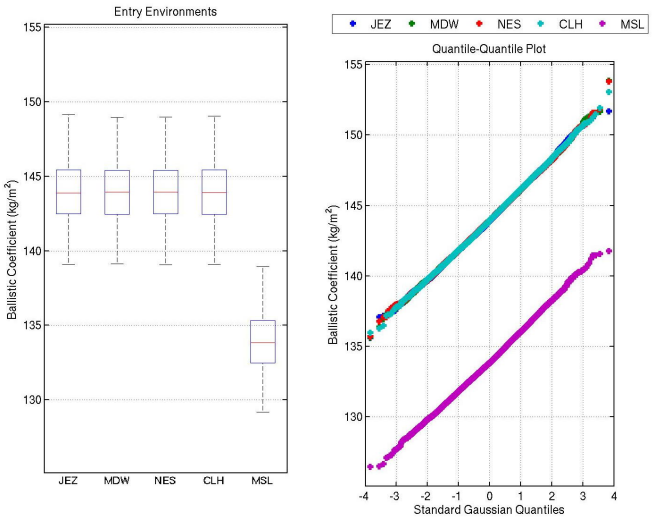

Figure 7. Comparison of hypersonic ballistic coefficient $(m/C_D A)$ at $Mach = 24$.

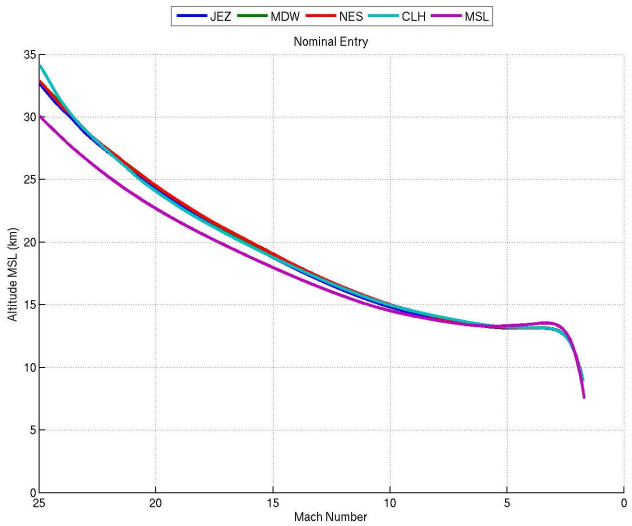

Figure 8. Comparison of nominal entry trajectories, Altitude vs. Mach number.

Atmospheric Entry

Traditionally at Mars, we define Entry Interface (EI) at a radius of $3522.2\ km$, which is $125\ km$ above the mean planet radius. Table 3 lists the mean EI conditions for Mars 2020. As noted previously, the mean entry mass of $3406\ kg$ is approximately $250\ kg$ more than MSL, an 8% increase. Figure 7 compares the hypersonic ballistic coefficient at Mach 24, which is approximately $145\ kg/m^2$ for Mars 2020.

Compared to MSL, the entry velocity is $400\ m/s$ slower at $5.4\ km/s$, a decrease of 7%. Combined with the increase in atmospheric density associated with the improvement in pressure cycle, the reduced velocity results in deceleration at slightly higher altitudes throughout the hypersonic portion of the entry, as shown in the nominal entry trajectory comparison in Figure 8. This figure also shows that all of the trajectories converge in the supersonic regime, resulting in very similar parachute deploy conditions, due to the active guidance system.

Figure 9 compares the peak deceleration, which is reduced by approximately 9% compared to MSL. In part, this reduction has allowed Mars 2020 to relax the Flight Limit Load (FLL) from $15\ g's$ to $12\ g's$, thus lowering acceptance test requirements on structural components of the flight aeroshell[5].

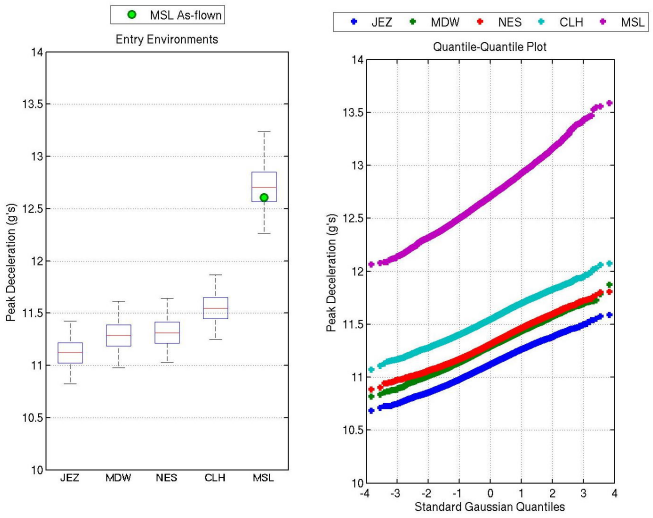

Figure 9. Comparison of peak deceleration during entry. Peak deceleration typically occurs at altitudes around $22\ km$.

Parachute Descent

Figure 10 is an image of MSL under parachute, captured by the High Resolution Imaging Science Experiment (HiRISE) camera aboard the Mars Reconnaissance Orbiter (MRO), during *Curiosity*'s parachute descent. Supersonic Disk-Gap-Band (DGB) parachutes have been operated successfully on Mars eight times, most recently by the Mars InSight lander. Even though these parachutes operated flawlessly on Mars, the Mars 2020 project became concerned about potentially low structural margins in the strength of the parachute following the failure of a parachute[6] during Low Density Supersonic Decelerator (LDSD) SFDT-2 flight test in June 2015. This

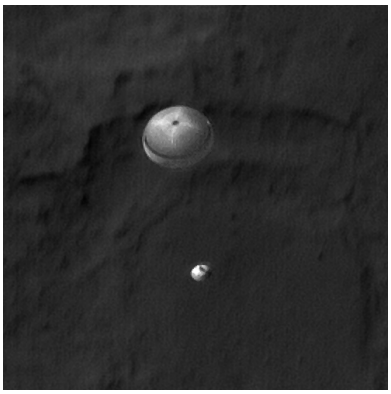

Figure 10. The High-Resolution Imaging Science Experiment (HiRISE) camera captured this image of *Curiosity* descending on parachute. Image Credit: NASA/JPL-Caltech/Univ. of Arizona.

[5]The relaxing of this requirement was motivated by the failure of the flight article during acceptance testing.

[6]The LDSD parachute was a 30 m ring sail, different in design from the 21.5 m MSL DGB.

Table 4. Mean Parachute Deploy (PD) Conditions

Parameter	Symbol	Value
Altitude	h_{PD}	8.7 km
Flight path angle	γ_{PD}	-17.6 deg
Velocity	V_{PD}	420.4 m/s
Mach number	M_{PD}	1.75
Dynamic pressure	q_{PD}	536.0 Pa

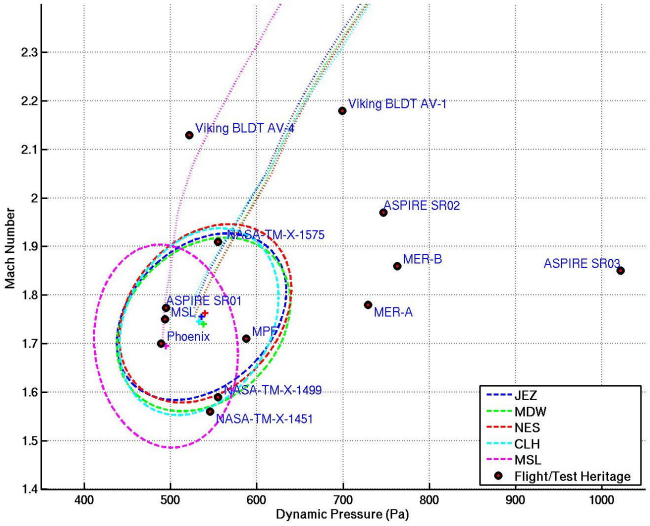

Figure 11. Comparison of parachute deploy conditions. Mach number vs. Dynamic Pressure.

concern prompted the project to redesign the Mars 2020 parachute with heavier broad-cloth materials and initiate a supersonic test campaign to qualify this stronger parachute. In response, the Advanced Supersonic Parachute Inflation Research Experiment (ASPIRE) program successfully tested three supersonic parachutes[7] at opening loads of 32, 56, and 67 thousand pounds, restoring confidence in the strengthened parachute design. [5] [6].

Table 4 lists the expected mean conditions at parachute mortar fire. Compared to MSL, these conditions are 0.05 higher in Mach number and only 40 Pa higher in dynamic pressure, which is due to Mars 2020's higher ballistic coefficient. Figure 11 compares parachute deployment conditions and places the 99%-tile Monte Carlo results in context with previous missions and test programs. Mean deployment conditions are very close to Mars Phoenix Lander, MSL, and ASPIRE SR-01 flights. The Mars 2020 range trigger produces slightly more eccentric ellipses in this plot due to the increased spread in velocity.

Figure 12 compares the peak opening load predictions using the momentum capture approach described in Way [4]. Due to the similarity of parachute deploy conditions, the mean expected opening load ($35,900$ $lbs.$) is only slightly higher than the MSL as-flown value of $34,600$ $lbs.$. Relative to the 99%-tile expected opening loads ($48,200$ $lbs.$), the largest of the ASPIRE tests, SR-03, at $67,000$ $lbs.$, represents approxi-

[7]SR-01 flew a build-to-print MSL parachute, while SR-02 and SR-03 flew the strengthened design. All three parachutes shared a common geometry and size to that of the MSL flight article.

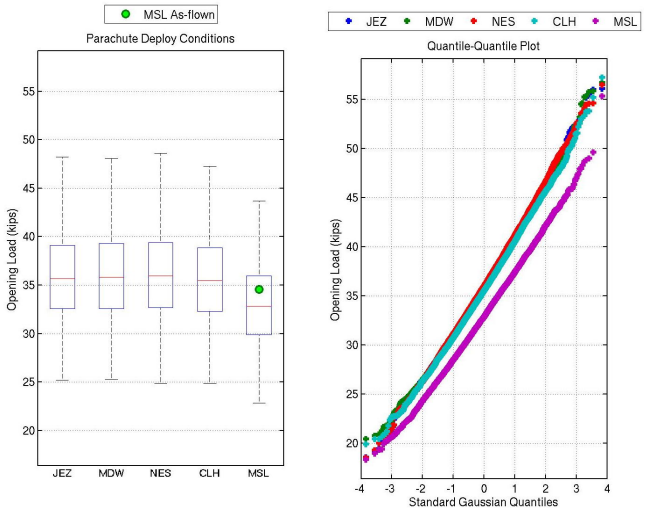

Figure 12. Comparison of peak parachute opening loads.

mately a 40% over-test of the flight system.

Timeline Margin

MSL carried only one sensor for real-time in-situ measurement of the surface of Mars: the Terminal Descent Sensor (TDS). Thus, EDL system timeline margin was defined as the elapsed time between achieving a valid altitude solution and the first timepoint in the sequence that requires that altitude measurement. For MSL, that first timepoint was the Mars Lander Engine (MLE) priming altitude of 3000 m AGL.

Mars 2020 will carry two in-situ sensors: the TDS and the LVS. Consequently, there are now two timeline margins that are important. As before, the first timeline margin is the one associated with the TDS altitude and velocity measurements. However, the first time that this solution is needed is now at 4200 m when the LVS begins to process descent images. Figure 13 compares this TDS timeline margin across the four landing sites. At all four landing sites, the 1%-tile margin is greater than 10 s.

The second timeline margin is associated with the LVS solution and its use within TRN. Similar to the definition of the TDS timeline margin, this new margin is defined as the elapsed time from the first valid LVS solution to the first time that solution is needed, which is when the divert decision is made at backshell separation. Figure 14 compares the TRN timeline margin. As with the TDS timeline margin above, the 1%-tile margin is greater than 10 s.

Therefore, considering the sum of the TDS and TRN timeline margins above, greater than 20 s of system-level timeline margin are available during parachute descent at a 99% confidence level. At the lowest elevation site, Jezero Crater, the mean timeline margin is 44.1 s. While at the highest elevation site, Columbia Hills, the mean timeline margin is 40.4 s. While some slight differences due to elevation are observable, less than 4 s of timeline margin separates all of the landing sites. Thus, timeline margin is not a key differentiator between landing sites.

Powered Descent

The powered descent sequence – from backshell separation through touchdown – is unchanged from MSL, with only a

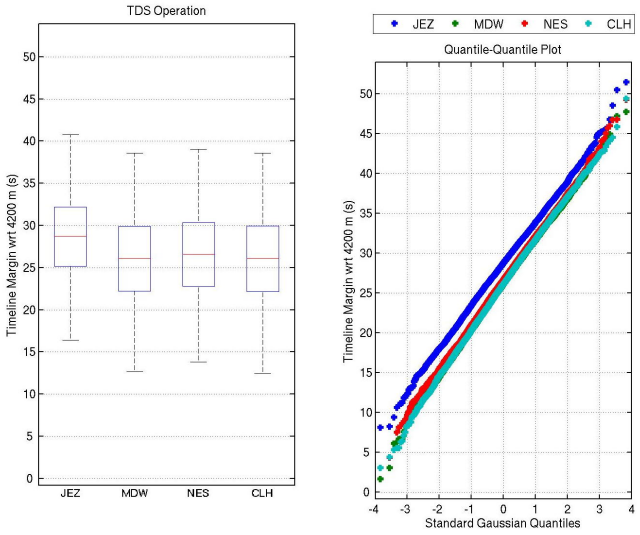

Figure 13. Comparison of Terminal Descent Sensor (TDS) timeline margin.

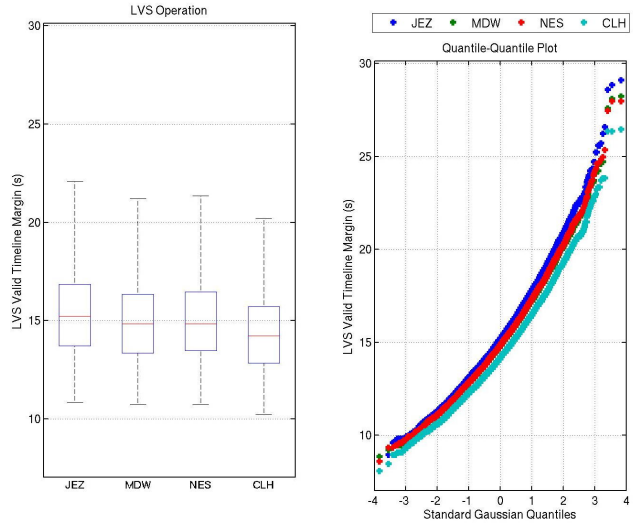

Figure 14. Comparison of Terrain Relative Navigation (TRN) timeline margin.

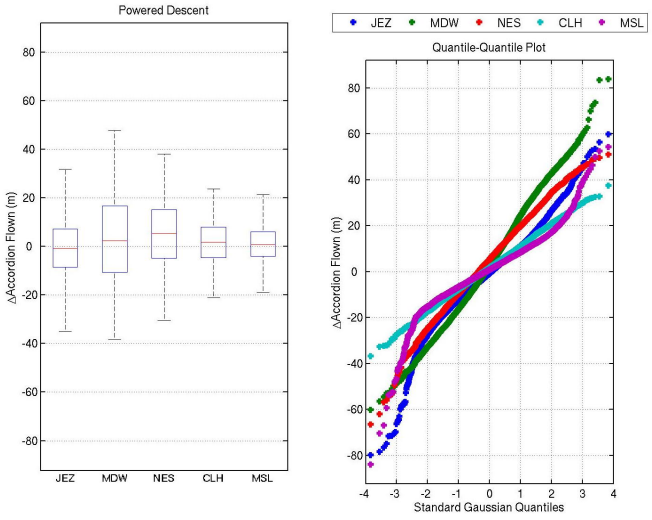

Figure 15. Comparison of the actual altitude difference, relative to the nominal set-point, flown during the constant velocity accordion.

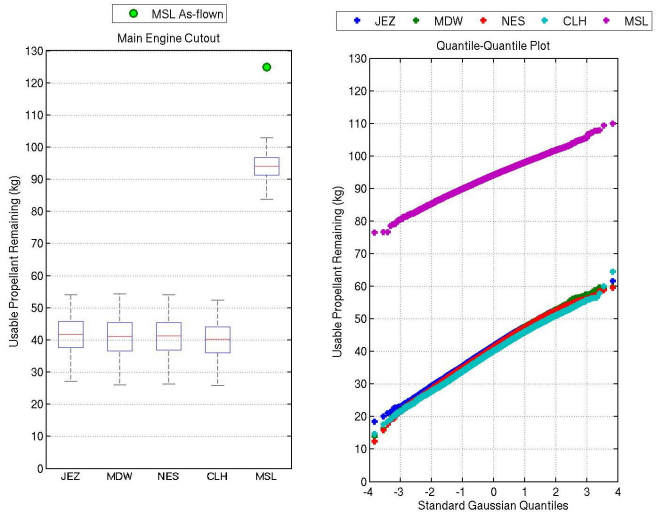

Figure 16. Comparison of useable propellant remaining after fly-away.

few parameter changes. For instance, backshell separation altitude for Mars 2020 has been raised 500 m higher than MSL, from 1800 m to 2300 m. This increase in altitude allows flying longer diverts with similar off-nadir angles. Larger off-nadir angles are avoided during the divert since they increase the chance of losing radar measurements, due to increasing both slant range and incidence angle. Additionally, the constant velocity accordion prior to landing has been increased from ± 100 m to ± 130 m to accommodate more terrain relief during the divert. Figure 15 compares the actual accordion flown at each site. This figure shows that the largest accordions at any site are approximately 80 m, well short of the 130 m allocation.

The primary resource expended in supporting the longer diverts for TRN is fuel. Figure 16 compares the useable propellant remaining after executing fly-away. This figure shows that, because of the longer divert distances required for TRN, Mars 2020 is using approximately 50 kg more fuel, on average, than MSL. Note that the disagreement between the "as-flown" reconstructed fuel use and the predicted fuel use for MSL is due to a conservative model of the Mars Lander Engine (MLE) specific impulse in the simulations. As this model has not been updated, it is expected that the Mars 2020 fuel estimates are similarly conservative.

6. Probability of Success

As can be seen in the previous section, the inclusion of the TRN subsystem has required only minor accommodations in EDL margins and consumables: an altitude solution is needed 1200 m higher than before, backshell separation has been tuned to occur 500 m higher, and powered approach diverts can be up to 335 m farther – requiring approximately 50 kg more propellant than before. Despite these accommodations, the EDL system remains robust and still maintains sufficient margins.

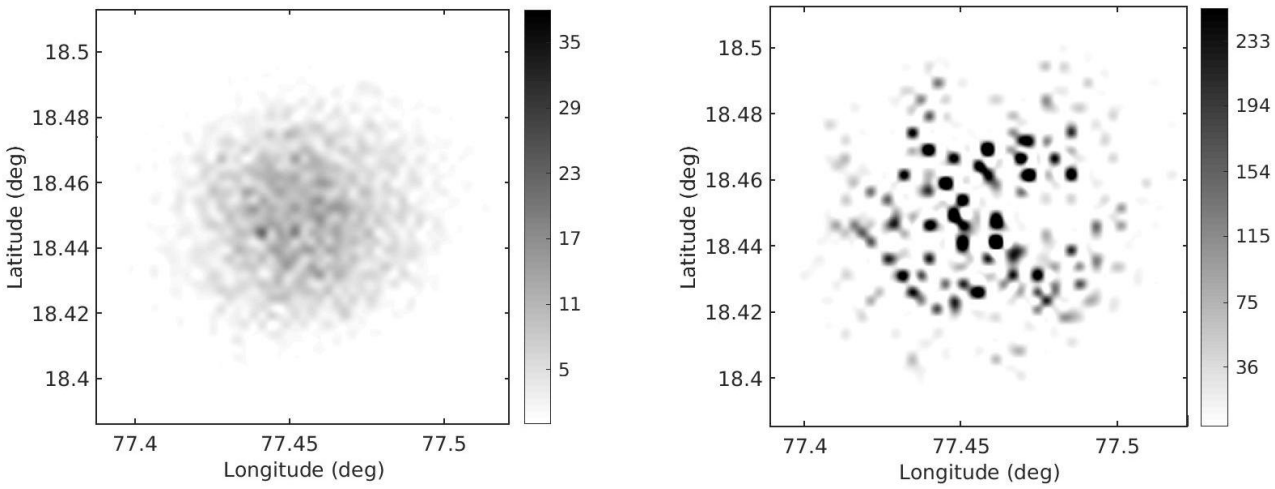

Figure 17. The panel on the left shows the frequency of backshell separation occurring within a 150 x 150 m grid. Without TRN, the landed points would have a similar bivariate Gaussian distribution. The panel on the right shows the landing points concentrating at safe locations, when utilizing the TRN system.

Table 5. Effect of TRN on Landed Slopes

Landing Site	99% Slope w/o TRN	99% Slope w/ TRN
JEZ	17.6°	8.2°
MDW	21.9°	11.4°
NES	20.2°	7.0°
CLH	10.1°	8.8°

Yet, the effect of TRN on the distribution of landing points within the ellipse is striking, as can be seen in Figure 17. In this figure, the spatial distribution of the backshell separation points is used as a proxy for landed locations without TRN. Without TRN, the cumulative affect of entry and parachute segment dispersions results in a continuous, approximately bivariate normal, distribution of landed points. With TRN, however, the the landing points are concentrated around local maxima in the STM safety levels. Since these safety levels incorporate the project's best estimates of hazards due to slopes, rocks, inescapable hazards, and CFA, the landing points are heavily biased towards locations where these hazards are minimized.

Table 5 provides the 99th percentile touchdown slopes encountered at each of the four landing sites, both with and without TRN. This table shows that the risk of landing on a high slope (slopes larger than 10 deg) is significantly reduced when using TRN. Likewise, Figure 18 compares the distribution of touchdown slopes across the four landing sites. In general, these distributions are similar across all four sites, though highest at Midway.

Table 6 provides the 99th percentile CFA encountered at each of the four landing sites, both with and without TRN. CFA is a measure of the residual risk of striking a smaller rock that was not identified in orbital imagery. This table shows that the risk of landing in a region with a high CFA is significantly reduced when using TRN. Likewise, Figure 19 compares the

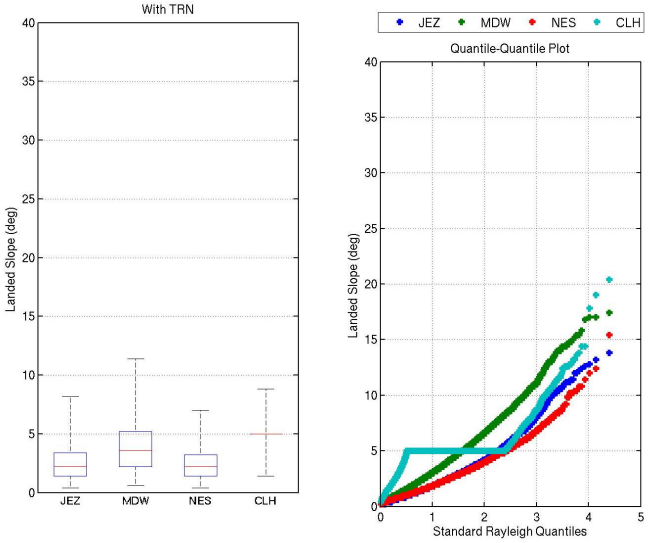

Figure 18. Estimated distribution of slopes at the touchdown location.

distribution of touchdown CFA across the four landing sites. In general, these distributions are less similar than the slopes in Figure 18, with the highest risk at Jezero.

The Mars 2020 TRN system is designed to bias the landed location away from known touchdown risks, including: slopes, large rocks identified from orbital imagery, inescapable hazards, and CFA. The STM accomplishes this by including the best estimate of the spatial distribution of these hazards and adding a padding function that accounts for the targeting accuracy of the EDL system. Table 7, provides the overall, integrated probability of success at each landing site, with and without TRN. In spite of large differences in the inherent risk of these landing sites, this table demonstrates that (with TRN) the overall probability of success is increased to approximately 99% for all of the candidates.

Table 6. Effect of TRN on Landed CFA

Landing Site	99% CFA w/o TRN	99% CFA w/ TRN
JEZ	18.8%	13.7%
MDW	22.8%	11.3%
NES	24.8%	6.6%
CLH	13.7%	9.2%

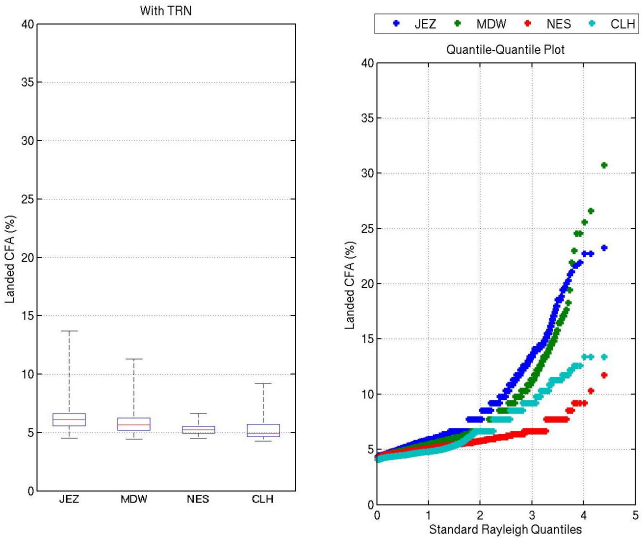

Figure 19. Estimated distribution of Cumulative Fractional Area (CFA) of rocks at the touchdown location. CFA is a measure of the residual risk of striking a smaller rock that was not identified in orbital imagery.

7. CONCLUSIONS

A key step in the development of the Mars 2020 mission is the selection of a suitable landing site with the largest likelihood of meeting scientific goals. This decision is a complex and critical one that requires close interaction between the scientific and engineering communities. The chosen landing site must be both scientifically interesting — providing the project with the greatest possible chance of gathering credible and defendable scientific evidence — and also safe enough to attempt a landing.

The culmination of the engineering effort to select the landing site is the Landing Site Safety Assessment. This review is commissioned by the project, and presided over by the EDL Standing Review Board. Attended by management and science stakeholders, the EDL team communicates their assessment of the associated landing risks and the statistical probability of a successful landing at each of the final four candidate landing sites: Jezero Crater, North East Syrtis, Midway, and Columbia Hills.

Table 7. Effect of TRN on Probability of Success

Landing Site	Footprint Size	Prob. w/o TRN	Prob. w/ TRN
JEZ	7.1 x 6.4 km	87.96%	98.77%
MDW	7.7 x 6.5 km	88.91%	99.12%
NES	7.3 x 6.4 km	94.00%	99.43%
CLH	7.0 x 6.3 km	97.53%	99.28%

This assessment relies heavily on computer simulations of the EDL sequence to predict vehicle performance and EDL system margins. Much of the Mars 2020 EDL system derives its heritage from the successful Mars Science Laboratory (MSL) landing, thus providing an excellent benchmark for Mars 2020 EDL system performance. Due in large part to the favorable pressure cycle in the 2020 arrival opportunity, the EDL system is able to carry more mass to a higher landing elevation. From an EDL performance perspective, all four candidates offer similar level of robustness. They all have similar altitudes with respect to the Mars areoid, and the EDL system has sufficient altitude and timeline margins.

Two new features of the Mars 2020 EDL sequence, range trigger and Terrain-Relative Navigation, dramatically enhance the capability of the EDL system to safely land at landing sites with much more rugged terrain than ever before considered. This has allowed the landing site selection for Mars 2020 to proceed in a manner that has been unprecedentedly weighted more heavily toward scientific interest and less heavily on engineering constraints. With TRN, the overall probability of success is predicted to be approximately 99% for all of the candidates.

On November 19, 2018, NASA announced that Jezero Crater had been selected as the landing site for the Mars 2020 rover. This announcement marked the end of a four-year process to choose where the rover will land when it arrives at Mars, February 18, 2021.

ACKNOWLEDGMENTS

The Mars 2020 rover mission is part of NASA's Mars Exploration Program, a long-term effort of robotic exploration of the Red Planet. The project is managed for NASA's Science Mission Directorate (SMD) by the Jet Propulsion Laboratory (JPL), a division of the California Institute of Technology.

Samalis Santini performed work for this paper under a NASA Space Technology Research Fellowship (NSTRF) grant, number 80NSSC17K0142, "Intelligent Data Understanding for Architecture Analysis of Entry, Descent, and Landing".

REFERENCES

[1] G. F. Mendeck and G. L. Carman, "Guidance Design for Mars Smart Landers Using the Entry Terminal Point Controller," AIAA 2002-4502, *AIAA Atmospheric Flight Mechanics Conference and Exhibit*, Monterey, CA, Aug 2002.

[2] D. W. Way, "On the use of a range trigger for the Mars Science Laboratory Entry, Descent, and Landing," IEEEAC 1142, *IEEE Aerospace Conference*, Big Sky, MT, Mar 2011.

[3] S. Dutta and D. W. Way, "Comparison of the Effects of Velocity and Range Triggers on Trajectory Dispersions for the Mars 2020 Mission," AIAA 2017-0245, *AIAA Atmospheric Flight Mechanics Conference*, Grapevine, TX, 2017.

[4] D. W. Way, "A Momentum-Based Method for Predicting the Peak Opening Load for Supersonic Parachutes," IEEEAC 2817, *IEEE Aerospace Conference*, Big Sky, MT, Mar 2018.

[5] C. O'Farrell, C. Karlgaard, J. A. Tynis, and I. G. Clark, "Overview and Reconstruction of the ASPIRE Project's SR01 Supersonic Parachute Test," *IEEE Aerospace Conference*, Big Sky, MT, Mar 2018.

[6] C. O'Farrell, B. Sonneveldt, C. Karlgaard, J. A. Tynis, and I. G. Clark, "Overview of the ASPIRE Project's Supersonic Flight Tests of a Strengthened DGB Parachute," *IEEE Aerospace Conference*, Big Sky, MT, Mar 2019.

[7] A. Nelessen, C. Sackier, I. Clark, P. Brugarolas, G. Villar, A. Chen, A. Stehura, R. Otero, E. Stilley, D. Way, K. Edquist, S. Mohan, Cj Giovingo, and M. Lefland, "Mars 2020 Entry, Descent, and Landing System Overview," *IEEE Aerospace Conference*, Big Sky, MT, Mar 2019.

BIOGRAPHY

David Way *is an Aerospace Engineer in the Atmospheric Flight and Entry Systems Branch at the NASA Langley Research Center. His area of expertise is flight mechanics and modeling and simulation of planetary entry systems. Dr. Way has a Ph.D. and M.S. in Aerospace Engineering from the Georgia Institute of Technology and a B.S. in Aerospace Engineering from the United States Naval Academy, Annapolis.*

Soumyo Dutta *is an Aerospace Engineer in the Atmospheric Flight and Entry Systems Branch at the NASA Langley Research Center. His current research focus is flight mechanics simulation and modeling of planetary entry systems. Soumyo has a Ph.D. and M.S. in Aerospace Engineering from the Georgia Institute of Technology and a B.S. in Mechanical Engineering from the University of Tennessee, Knoxville.*

Carlie Zumwalt *is a member of the Atmospheric Flight and Entry Systems Branch at the Langley Research Center. She received her Bachelor's degree in aerospace engineering from the University of Texas at Austin in 2009 and joined the Johnson Space Center as a flight mechanics engineer before transferring to Langley. Over her ten year career she has been involved in projects ranging from human Mars explorations studies to parachute wind tunnel testing, and is currently supporting InSight, Mars 2020 and the Commercial Crew program.*

Samalis Santini *received her B.S in Mechanical Engineering from the University of Puerto Rico at Mayaguez in 2016 and her M.S. in Aerospace Engineering at Cornell University in 2018. She is currently a Ph.D. graduate student at Texas A&M University in the Aerospace Engineering department and is a part of the Systems Engineering, Architecture, and Knowledge (SEAK) Lab. Her interests are the application of statistical learning and knowledge extraction techniques for architecture analysis of Entry, Descent, and Landing (EDL) Systems.*